Comparison of 22 kHz and 85 kHz 50 kW Wireless Charging System Using Si and SiC Switches for Electric Vehicle

Moinul Shahidul Haque
Dept. of Electrical and Computer Engineering, Mississippi State University,
Starkville, MS, USA
mh3273@msstate.edu

Mostak Mohammad
Dept. of Electrical and Computer Engineering, University of Akron,
Akron, OH, USA
mm251@zips.uakron.edu

Jason L. Pries
National Transportation Research Center, Oak Ridge National Laboratory, Oak Ridge, TN, U SA
priesjl@ornl.gov

Seungdeog Choi
Dept. of Electrical and Computer Engineering, Mississippi State University,
Starkville, MS, USA
s.choi@msstate.edu

***Abstract*—Fast charging in transportation application requires high-power (>50 kW) operation. The overall size of wireless charging systems (WCS) must increase to meet the high-power requirement. As a result, high power systems produce more electromagnetic field (EMF) emissions. Although higher operating frequencies (85 kHz) reduce the size of inductors and capacitors, system losses tend to increase. High-power systems are traditionally investigated for 10 kHz to 22 kHz operation to reduce the switching loss in the converter, and conductive and magnetic losses in the power pad. The use of SiC MOSFETs reduces conduction and switching losses in the converter even at higher frequencies. In this paper, a comprehensive loss comparison of 50 kW wireless charging system is conducted for 85 kHz and 22 kHz operation of Si MOSFET and SiC MOSFET converters. Detailed performance indexes are compared analytically as a function of frequency and verified using FEA and PLECS. This comprehensive system level study shows that magnetic losses can be reduced significantly, and that EMF emission can be reduced by 50% by moving from 22 kHz to 85 kHz. Moreover, the system requires 50% less copper and allows a significant reduction in the size of the primary and secondary filter capacitor at 85 kHz. The results show that the system efficiency at 85 kHz can be increased by 21% compared to 22 kHz operation by using a SiC MOSFET converter.**

Keywords—Inductive charging, Core loss, Shield loss, Litz-wire, EMF suppression.

I. INTRODUCTION

WIRELESS charging systems (WCS) have become a potential alternative for charging at home and on the road. This technology has been investigated widely in last three decades for systems ranging from 3kW to 10kW and has shown significant efficiency and performance improvements while operating safely and reliably [1-3]. The technology is on the verge of commercialization and the Society of Automotive Engineers (SAE) has already published standard system configuration recommendation for systems up to 11kW with greater than 90%. Although light duty (LD) applications have achieved significant technological maturity, heavy duty (HD) charging systems (>20kW) are still being developed and optimized for size, geometry, coil configuration, and frequency range.

Additionally, HD systems also lack guidelines stemming from comprehensive analysis [2]. In this paper, a HD WCS is investigated using analytical methods focusing on the choice of operating frequency and the effect of traditional Si switches versus SiC switches on system performance at those frequencies.

The system components of an EV WCS are shown in Fig.1. High-power designs require more amp-turns in the transmission (Tx) and receiving (Rx) coils, increasing conduction losses [4-5]. High-power systems also require physically larger inductors and capacitors when the system is designed for lower frequencies such as 22 kHz. The size of the inductors and capacitors can be reduced when the system operates at higher frequencies such as 85 kHz. However, the switching losses of converters with traditional Silicon MOSFETs increas significantly at 85 kHz. These losses limit the choice of switching circuit and magnetic pad components due to switching frequency and power handling limitations. Low power (e.g., 3.7kW, 7.7kW and 11.0kW) systems have been standardized to operate at 85 kHz [6]. However, high power systems do not have such standardization to date [7].

With the introduction of wide bandgap materials such as Silicon Carbide (SiC) in power semiconductor, overall switching losses can be reduced at high frequency and in high power applications. In addition to lower switching energy loss, SiC MOSFETs have 27% lower $R_{DS,ON}$ compared to similar Si MOSFETs [8,9]. For this reason, SiC MOSFETs based converters have lower losses than Si MOSFETs based ones. Lower converter losses raise the following questions: Can system-level losses of WCS at 85 kHz be reduced? If so, what system levels design opportunities and trade-offs exist for this operating frequency?

The paper is organized as follows: In Section II, characteristics of different system losses are investigated and their relation

This manuscript has been partially authored by UT-Battelle, LLC under Contract No. DE-AC05-00OR22725 with the U.S. Department of Energy. The United States Government retains and the publisher, by accepting the article for publication, acknowledges that the United States Government retains a non-exclusive, paid-up, irrevocable, world-wide license to publish or reproduce the published form of this manuscript, or allow others to do so, for United States Government purposes. The Department of Energy will provide public access to these results of federally sponsored research in accordance with the DOE Public Access Plan (http://energy.gov/downloads/doe-public-access-plan). A portion of this research used resources at the Power Electronics and Electric Machinery Research Facility, a DOE Office of Science User Facility operated by the Oak Ridge National Laboratory.

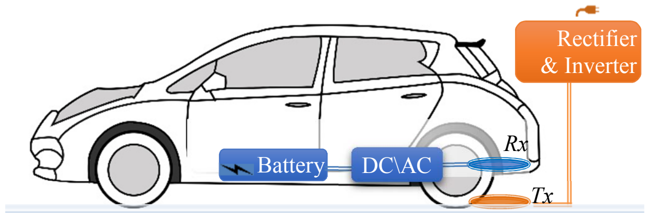

Fig. 1: Basic system components of EV wireless charging system.

ship with frequency is presented. In Section III, Si and SiC inverters are investigated for 50 kW WCS through FEA and PLECS based circuit analysis and the results are compared for 85 kHz and 22 kHz.

II. Performance of Wireless Charging System

Fig.2. shows a WCS having a DC source cascaded with an inverter, a resonant tank, a rectifier, and a load. Different resonant tank topologies are used in WCS. In this paper, a series-series resonant tank is used for wireless power transfer. Due to low equivalent series resistance (ESR), the tuning capacitor are assumed ideal. The loss elements in WCS are divided into two groups: 1) converter, and 2) resonant tank. The efficiency of the WCS is determined by the losses in the semiconductor switches in the primary side inverter and secondary side rectifier, and the losses in coil, core, and shield of the transmitter and receiver:

$$P_{loss} = P_{switching} + P_{conduction} + P_{coil} + P_{core} + P_{shield} \quad (1)$$

where P_{loss} is the total loss of the WCS, $P_{switching}$ is the switching loss of MOSFET and diode in the converter, $P_{conduction}$ is the conduction loss of MOSFET and diode in the converter, P_{coil} is the conduction loss of primary and secondary coils, P_{shield} is the eddy current loss in the shield, and P_{core} is the loss in the magnetic core. $P_{switching}$ depends on the operating frequency and constituent material of the semiconductor switches. $P_{conduction}$ depends on the intrinsic material property of the switch. P_{coil}, P_{shield}, and P_{core} show a nonlinear relationship with the operating frequency due to the skin effect in conductors and hysteresis phenomena in ferrites. P_{core} also shows a nonlinear relation with flux density. The frequency dependence of the coil can be reduced using Litz wire. Throughout this paper, operating frequency and switching frequency will be used interchangeably. Detailed loss characteristics of these groups are analyzed in the following sub-sections:

A. Performance and Loss Characterisitics of Magnetic Pad

The total power transferred from the transmitter to the receiver coil is expressed as follows:

Table I
Components Used in This Study

Components	Specification
Si MOSFET	APTC60AM18SCG
SiC MOSFET	CAS120M12BM2
Rectifier Diode	CAS120M12BM2-Body Diode
Litz Coil	4125×AWG38 for 85kHz 1650×AWG34 for 20kHz
Shield	Aluminum 6101 Alloy
Ferrite Core	Feroxxcube-C95

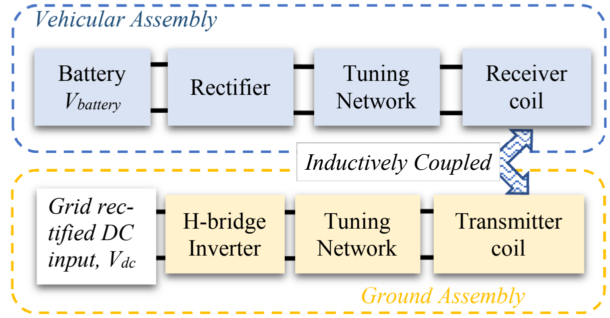

Fig. 2. Fundamental power processing units of wireless charging system.

$$P = \omega M I_{tx} I_{rx}^{*} = 2\pi f k \sqrt{L_{tx} L_{rx}}\, I_{tx} I_{rx}^{*} \quad (2)$$

where I_{tx} and I_{rx} are the transmitter and receiver coil currents, f is the operating frequency, L_{tx} and L_{rx} are the pad self-inductances, M is the mutual inductance, and k is the coupling coefficient. Equation (1) can be further elaborated as follows:

$$P = 2\pi f k (N_{tx} I_{tx})(N_{rx} I_{rx}^{*}) \sqrt{\hat{L}_{tx} \hat{L}_{rx}} \quad (3)$$

where $\hat{L}_{tx}$ and $\hat{L}_{rx}$ are the average inductance-per-turn of the transmitter and receiver coil, respectively. For a series-series compensated system, the transmitter and receiver currents can be defined as follows [15]:

$$I_{tx} = \frac{2\sqrt{2}}{\pi} \frac{V_{battery}}{\omega M} \text{ and } I_{rx}^{*} = \frac{2\sqrt{2}}{\pi} \frac{V_{dc}}{\omega M} \quad (4)$$

where $V_{battery}$ is the output battery voltage and V_{dc} in the DC voltage at the input of the inverter. The parameters k, $\hat{L}_{tx}$, and $\hat{L}_{rx}$ depend on the overall size of the coil and core, and are invariant with the number of turns in the coils when the turns are placed in such a way as to occupy the same cross-sectional area. Both I_{tx} and I_{rx} are determined by the input voltage, output voltage, and ωM (or $f N_{Tx} N_{rx}$). For this reason, I_{tx} and I_{rx} are considered constant for a certain power when the input-output voltage and $f N_{Tx} N_{rx}$ remains constant. Therefore, to transmit a fixed output power for fixed input and output voltage, pad size, and air-gap, the design must satisfy the following condition,

$$f N_{tx} N_{rx} = C_{fN} \quad (5)$$

where C_{fN} is a constant determined from (3) which is defined as follows:

$$C_{fN} = \frac{4}{\pi^3} \frac{V_{dc} V_{battery}}{P k \sqrt{\hat{L}_{tx} \hat{L}_{rx}}}$$

This constraint relating the frequency to the number of turns makes it possible to perform a comprehensive analysis of the coil losses, core losses, and shield losses with respect to the operating frequency. For the simplicity of the analysis, the transmitter and the receiver are assumed to be matched coil with $N_{tx}=N_{rx}=N_f$ and $\hat{L}_{tx} = \hat{L}_{rx} = \hat{L}_{coil}$. From (5), the relation between the required number of turns at two different frequencies for a matched transmitter and receiver is as follows:

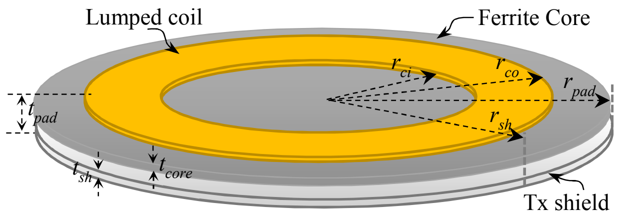

Fig.3. Basic components of a circular wireless charging pad showing lumped coil, ferrite core and aluminum shield.

$$\frac{N_{f_1}}{N_{f_2}} = \sqrt{\frac{f_2}{f_1}} \tag{6}$$

where N_{f1} and N_{f2} are the required number of turns at f_1 and f_2. For f_1=22 kHz and f_2=85 kHz, the relation is as follows:

$$\frac{N_{85kHz}}{N_{22kHz}} = \sqrt{\frac{22}{85}} = 0.5 \tag{7}$$

The number of turns required for 85 kHz is about half that of 22 kHz. The two different frequencies also require litz wire utilizing two different AWG strands. The magnetic materials of the charging pads, the number of turns, and the selection of switches in the converters are important for efficient operation at each of these frequencies. To observe the loss dependence on frequency, the most suitable components are chosen from a system level analysis. The quantitative data for the component set are given in Table I.

B. Magnetic Losses in WCS

As shown in Fig. 3, the charging pad has three main components: the coil, the core, and the shield. Losses in each of these components depend on the volume and electrical properties of the materials used, the number of turns in the coil, and the operating frequency. As the number of turns depends on f, the magnitude of the losses also significantly depends on f. The coil turn-number, N_f, is designed for a particular frequency and the resulting losses are investigated.

1) Comparison of Coil Losses

The coil losses depend on the ac resistance of the coil, R_{coil}, and current through it,

$$P_{coil} = I_{coil}^2 R_{coil} \tag{8}$$

The coil resistance can be expressed in terms of number of turns as

$$R_{coil} = \hat{R}_{coil} N_f \tag{9}$$

where $\hat{R}_{coil}$ is the average per-turn resistance of the coil which is dependent on frequency. Since the coil currents remain the same at two different frequencies, the coil losses are related as follows:

$$\frac{P_{coil-f_1}}{P_{coil-f_2}} = \frac{\hat{R}_{coil-f_1}}{\hat{R}_{coil-f_2}} \times \frac{N_{f_1}}{N_{f_2}} \tag{10}$$

Litz wire with suitable strand sizes must be selected for f_1 and f_2 to mitigate the skin effect. Additionally, the bundle size (total equivalent AWG size) of the litz wire must be the same to meet the current requirements. Therefore, the ratio of $\hat{R}_{coil\text{-}f_1}$ to $\hat{R}_{coil\text{-}f_2}$ should be approximately 1. For example, a strand size of 34 AWG is used at 22 kHz and 38 AWG is used at 85 kHz. For the same current capacity litz wire, the ratio of resistance per-unit-length is 64.8/65.3≈1. Therefore, substituting (6) into (9), the ratio of the coil losses at 22 kHz and 85 kHz is estimated as follows:

$$\frac{P_{coil-85kHz}}{P_{coil-22kHz}} \approx \sqrt{\frac{22}{85}} = 0.5 \tag{11}$$

Based on (10), the required coil length and consequent coil resistance can be reduced by approximately 50% for at 85 kHz system compared to a 22 kHz operation.

2) Comparison of Core Losses

The core loss at any point in the core can be estimated using Steinmetz equation as follows:

$$P_{core} = K_h f^{\alpha} B^{\beta} \tag{12}$$

where, K_h, α, and β are constants, and B is the flux density in the core. As B is proportional to NI, the ratio of P_{core} is written at two different frequencies as follows:

$$\frac{P_{core-f_1}}{P_{core-f2}} = \left(\frac{f_1}{f_2}\right)^{\alpha} \left(\frac{N_{f_1}}{N_{f_2}}\right)^{\beta} \tag{13}$$

Equations (12) and (13) show that, although the frequency dependent core loss in Steinmetz equation increases at higher frequency, the reduced number of turn and consequent reduced flux density in the core compensates that effect. Equation (13) can be further simplified using (6) as follows:

$$\frac{P_{core-f_1}}{P_{core-f2}} = \left(\frac{f_1}{f_2}\right)^{\alpha-\frac{\beta}{2}} \tag{14}$$

Typically, α varies between 1 and 1.5 and β varies between 2 and 2.7. Parameters for two different ferrite materials are shown in Table II [13,14]. Depending on the Steinmetz coefficients, the core losses can be reduced by 10% to 25% in an 85 kHz system compared to a 22 kHz system. For example, in FDK6H40 the core losses increase by 4% at 85 kHz, while in Ferroxcube-C95, they decrease by 21%.

TABLE II
STEINMETZ COEFFICIENTS

Core Model	K_h	α	β
Ferroxcube-C95	93	1.045	2.44
FDK-6H40	2.03	1.41	2.75

3) Comparison of the Shield Losses

Compared to the conductor losses, the shield loss characteristic shows a different relationship with frequency. As the shield acts as a single loop inductor [9], the shield losses are determined by the total ampere-turns in the coil and the equivalent shield resistance as follows:

TABLE III
GEOMETRIC PARAMETER OF THE STUDIED CIRCULAR PAD

Parameter	Nominal value
Coil outer radius	250 mm
Coil inner radius	150 mm
Number of turn for 22 kHz	12
Number of turn for 85 kHz	6
Air-gap	150 mm
Ferrite core radius	300 mm
Ferrite core thickness	5 mm
Aluminum shield thickness	3 mm
Aluminum shield radius	305 mm

$$P_{shield} = I_{shield}^2 R_{shield} \tag{15}$$

where I_{shield} is the shield current and R_{shield} is the equivalent shield resistance. R_{shield} depends on the skin depth of the conductor material. The skin depth at frequency f is as follows:

$$\delta = \sqrt{\frac{\rho}{\pi\mu f}} \tag{16}$$

where ρ is the resistivity of the material and μ is the permeability of the material. As ρ and μ are constant, the relationship between frequency and equivalent shield resistance is as follows:

$$R_{shield} \propto \frac{1}{\delta} \propto \sqrt{f} \tag{17}$$

I_{shield} depends on the EMF induced in the shield and the equivalent impedance of the shield current path. The shield behaves as an inductor with series resistance R_{shield}. The shield current can be given as

$$I_{shield} = \frac{-\omega M_{shield-coil} I_{coil}}{j\omega L_{shield} + R_{shield}} \approx \frac{-M_{shield-coil} I_{coil}}{jL_{shield}} \tag{18}$$

where $M_{shield\text{-}coil}$ is the mutual inductance between the main coil and shield plate. As the shield is effectively a single-loop-inductor with constant shield inductance L_{shield}, $M_{shield\text{-}coil}$ is as follows:

$$M_{shield-coil} \approx k_{shield-coil} \sqrt{L_f L_{shield}} = k_{shield-coil} N_f \sqrt{\hat{L}_{coil} L_{shield}} \tag{19}$$

from (18) and (19), the relationship between the shield current and operating frequency is given as follows:

$$I_{shield} \propto N_f \tag{20}$$

The ratio of the shield loss for f_1 and f_2 is as follows:

$$\frac{P_{shield-f_1}}{P_{shield-f_2}} = \left(\frac{I_{shield-f_1}}{I_{shield-f_2}}\right)^2 \left(\frac{R_{shield-f_1}}{R_{shield-f_2}}\right) \tag{21}$$

Using (6), (20), and (21), this relation can be simplified as follows:

$$\frac{P_{shield-f_1}}{P_{shield-f_2}} = \left(\frac{N_{f_1}}{N_{f_2}}\right)^2 \sqrt{\frac{f_1}{f_2}} = \sqrt{\frac{f_2}{f_1}} \tag{22}$$

which indicates that, like the coil loss, the shield loss can be reduced by 50% when moving from 22 kHz to 85 kHz operation.

4) Comparison of Emissions Characteristics

According to the proposed SAE standard J2954 on wireless charging, the electromagnetic fields (EMF) must be limited both inside and outside the vehicle. The maximum magnetic field in publicly accessible area should be lower than 27 μT_{rms} for frequencies in the 3kHz to 100 kHz range. At 50 kW, the system will emit more EMF and shielding becomes more challenging. The EMF depends on the primary and secondary ampere-turns and their phase difference. At resonance, the phase difference between the primary and secondary coil currents is 90 degrees. The leakage magnetic field at any point varies as follows:

$$B_{leakage-f} \propto N_f I \tag{23}$$

Therefore, at two different frequencies, considering the respective number of turns in each coil, the leakage flux is as follows:

$$\frac{B_{leakage-f_1}}{B_{leakage-f_2}} = \frac{N_{f_1}}{N_{f_2}} = \sqrt{\frac{f_2}{f_1}} \tag{24}$$

Equation (24) indicates that, compared to a 22 kHz system, the EMF emission are reduced to half in an 85 kHz system.

FEA analysis-based comparison of different magnetic losses and EMF emission for the 85 kHz and 22 kHz systems for 50 kW power transfer are given in Table IV. Its shows that,

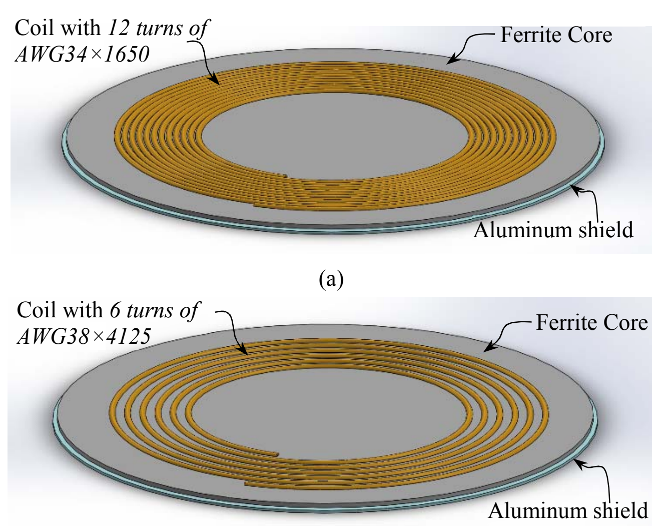

Fig. 4: The FEA model of (a) 22kHz and (b) 85 kHz 50kW wireless charging pad having same size of coil core and shield with 12 and 6 turns, respectively.

TABLE IV
MAGNETIC LOSS COMPARISON FOR 50 KW AT V_{dc}=$V_{battery}$= 650V

Loss	22kHz System	85kHz System
Coil loss, P_{coil}	151.4 W	78.6 W
Core (Feroxxcube-C95) loss, P_{core}	153.9 W	116.4 W
Shield loss, P_{shield}	176.0 W	90.3 W
Leakage Magnetic Field at SAE recommended 0.8m from Rx center	44.2 µT	22.1 µT

compared to the 22 kHz system, in 85 kHz system the coil and the shield losses are reduced by 50%, and the core loss for Feroxxcube-C95 core has been reduced by 24%, the total copper required in the coil has been reduced by 50%. More importantly, magnetic flux leakage for 22kHz system is 44.2 μT, which exceeds the ICNIRP limit of 27 μT at publicly exposed area. This leakage flux in the 85 kHz system has been reduced by 50% and under the limit of ICNIRP.

C. Inverter and Rectifier Losses in WCS

The circuit diagram of a WCS is shown in Fig. 5. The inverter and rectifier are important components in the WCS. The inverter converts DC into AC on the transmitter side while the rectifier converts AC to DC on the receiver side. The main components are MOSFETs in the inverter and diodes in rectifier. Understanding the individual loss mechanism in MOSFETs and diodes provides better insight about loss estimation for these two converter systems.

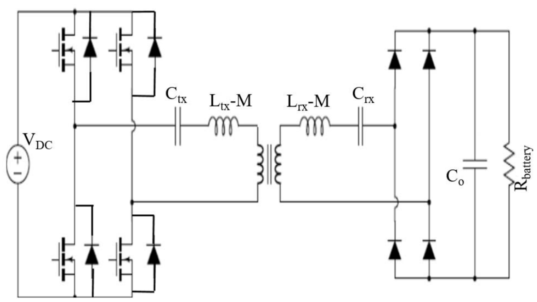

Fig. 5. Fundamental DC-to-DC circuit diagram of a wireless charging system.

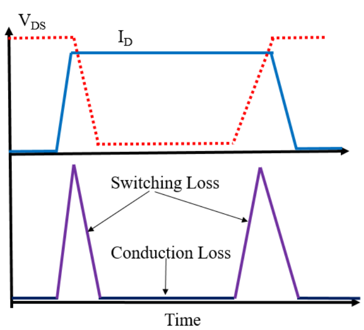

Fig. 6. Loss incurred in a MOSFET during the switching and conduction period.

1) Analytical Loss Modeling of MOSFET

Power semiconductor switching losses are crucial for converter design as they are the dominant factor in efficient thermal management of the system. The operating frequency of the converter is limited by losses in the switches. Losses in a MOSFET are categorized as conduction losses, switching losses, and leakage losses [10-12]. Leakage losses are negligible compared to conduction losses and switching losses.

The existence of non-zero on-state drain-source voltage ($V_{DS,ON}$) results in conduction losses. This on-voltage is approximated by the product of an on-state resistance ($R_{DS,ON}$) and drain current (I_D). $R_{DS,ON}$ is defined as the ratio of on-voltage and on-drain current. The average conduction loss over a period is as follows:

$$P_{c-MOS} = R_{DS,ON} I_{Drms}^2 \tag{25}$$

where $P_{c\text{-}MOS}$ is the MOSFET conduction loss and I_{Drms} is the root mean square drain current. These conduction losses do not depend on frequency. This loss component is expected to be the same at 22 kHz and 85 kHz. It is dependent on the constituent material of the MOSFET. As SiC has lower $R_{DS,ON}$ compared to Si, the conduction loss of SiC MOSFETs are lower. $R_{DS,ON}$ is temperature dependent and assumed constant at steady state.

In an ideal MOSFET, the transition of V_{DS} and I_D are instantaneous and results in no switching loss. However, the actual voltage and current transitions take finite time and results in significant switching losses in real MOSFETs as shown in Fig.6. The switching loss has two components; turn-on and turn-off loss. The magnitude of these losses are related to the rise and fall time of V_{DS} and I_D. The turn-on energy loss of MOSFET is as follows:

$$E_{On-MOS} = V_{DD} I_{D,on} \frac{t_{ri} + t_{fu}}{2} + Q_{rr} V_{DD} \tag{26}$$

where, $E_{on\text{-}MOS}$ is the MOSFET on energy, V_{DD} is the voltage of the DC source, t_{ri} is the rise time of I_D, t_{fu} is the fall time of V_{DS}, and Q_{rr} is the reverse recovery charge of the free-wheeling diode. The turn-off loss does not have a reverse recovery phenomenon and is calculated as follows:

$$E_{off-MOS} = V_{DD} I_{Doff} \frac{t_{ru} + t_{fi}}{2} \tag{27}$$

where t_{fi} is the fall time of I_D and t_{ru} is the rise time of V_{DS}. The switching losses of the MOSFET are calculated as follows:

$$P_{sw\_MOS} = \left(E_{on\_MOS} + E_{off\_MOS} \right) f \tag{28}$$

where $P_{sw\text{-}MOS}$ is the MOSFET switching losses and f is the switching frequency of system.

The aforementioned rise and fall times depend on $R_{DS,ON}$, gate resistance (R_g), and gate to drain capacitance of the MOSFET. These parameters are different for Si and SiC MOSEFTs, resulting in different switching losses. For a MOSFET, E_{on} and E_{off} remain constant for a given operating condition. The relation between switching losses and operating frequency is as follows:

$$\frac{P_{sw\_MOS,f_1}}{P_{sw\_MOS,f_2}} = \frac{f_1}{f_2} \tag{29}$$

When the operating frequency increases from 22 kHz to 85 kHz, the switching loss is expected to increase four times.

2) Analytical Loss Modeling of Diodes

Inverter MOSFETs have antiparallel diodes to accommodate inductor currents when the MOSFET is turned off. The conduction losses of the diode are calculated as follows:

TABLE V

DESIGNED SYSTEM PARAMETER

Output power	50 kW	
Input voltage, V_{dc}	650 V	
Output voltage, $V_{battery}$	650 V	
MOSFET Gate resistance	2.5Ω	
Operating frequency, f	22 kHz	85 kHz
Number of turn, N_{tx}=N_{rx}	12	6
Mutual Inductance, M	51 µH	13 µH
Self-Inductance, L_{tx}=L_{rx}	140 µH	37 µH
SS compensation capacitance, C_{tx}=C_{rx}	0.37 µF	95 nF

$$P_{c-Diode} = V_{D0} I_{Fav} + R_D I_{Frms}^2 \quad (30)$$

where I_{Fav} is the average diode current, I_{Frms} is the RMS diode current and R_D is the on resistance of the diode. The diode conduction loss is frequency-independent and the same at 22 kHz and 85 kHz. Like MOSFETs, the diode switching losses also have two components; turn-on and turn-off loss. As turn-off losses in the diode are neglected, the switching losses are estimated as follows:

$$P_{sw-Diode} = E_{on\_Diode} f_{sw} = \frac{1}{4} Q_{rr} V_{Drr} f_{sw} \quad (31)$$

where V_{Drr} is the reverse recovery voltage of diode. The reverse recovery charge of the MOSFET is very low for SiC schottky diodes. For this reason, the switching losses in the diodes are negligible.

The total losses in the WCS converts is the sum of conduction and switching losses in four MOSFETs, their antiparallel diodes in the inverter, and four rectifier diodes.

III. SIMULATION AND COMPARISON

A detailed PLECS based simulation was conducted for a 50 kW, 650 V system. The system parameters are given in Table V. The system is simulated in both the phase-shifted full bridge (PSFB) zero-voltage switching (ZVS) condition and the hard-switching condition. The system is operated slightly inductive rather than resistive under PFSB-ZVS condition. This adjustment is made to achieve ZVS. The advantage of ZVS is to reduce the turn-on losses in the MOSFETs. The switching frequencies are 22.5 kHz and 88.5 kHz respectively for both the Si and SiC MOSFET based systems. Losses in the inverter and rectifier under these conditions are in given in Table VI and Table VII.

With hard switching at 22 kHz, the total efficiency of the system is 99.03% for Si MOSFETs and 99.41% SiC MOSFETs. The efficiency drops to 98.57% and 99.22% respectively at 85 kHz due to an increase in switching losses. The switching losses in the Si and SiC based systems increases almost four times when the operating frequency changes from 22 kHz to 85 kHz as predicted by (29). However, the conduction losses remain almost constant when frequency is changed from 22 kHz to 85 kHz. When the Si MOSFETs are replaced by SiC MOSFETs, the conduction losses in the system is reduced by almost 75%. The improved efficiency of the SiC MOSFET converter under FBPS-ZVS is due to significantly lower conduction losses. The efficiency of the system increases 1.25% when SiC MOSFETs are used.

TABLE VI

LOSS COMPARISON OF SI AND SIC MOSFETS UNDER THE *HARD-SWITCHING* CONTROL

Switching frequency (kHz)	22 kHz		85 kHz	
MOSFET and diode Type	Si	SiC	Si	SiC
MOSFET switching losses (W)	63.48	31.14	230.6	105.9
MOSFET conduction losses (W)	262.9	64.5	272.1	68.9
Diode conduction losses (W)	214.5	214.6	214.5	214.4
Total loss (W)	540.9	310.2	717.2	389.2
Efficiency (%)	99.03	99.41	98.57	99.22

TABLE VII

LOSS COMPARISON OF SI AND SIC MOSFETS UNDER THE *SOFT-SWITCHING* CONTROL

Switching frequency (kHz)	22 kHz		85 kHz	
MOSFET and diode Type	Si	SiC	Si	SiC
MOSFET switching losses (W)	14.34	15.14	50.56	61.96
MOSFET conduction losses (W)	254.1	64.52	272.2	68.9
Diode conduction losses (W)	214.3	214.6	214.5	214.4
Total loss (W)	482.7	294.3	537.3	345.3
Efficiency (%)	99.03	99.41	98.93	99.31

IV. CONCLUSION

In this paper, a 50 kW wireless charging system for EV charging applications operating at 22kHz and 85kHz was investigated for Si and SiC MOSFET based converters. The system and its components are optimally designed for the two target frequencies and consequent losses are evaluated analytically, through FEA, and circuit analysis. The results show that, contrary to common perception, the overall magnetic losses decrease significantly at 85 kHz for charging pads of fixed size. Using SiC switches, it is shown that the switching losses decrease by 28% compared to Si MOSFETs during hard switching. Therefore, the SiC MOSFET and diode losses at 85 kHz increases by 465W compared to 565 W in the Si MOSFET system. In total, the losses in the 85 kHz wireless charging system reduces by 21% compared to the 22 kHz system.

REFERENCES

[1] J. Deng, W. Li, T. D. Nguyen, S. Li and C. C. Mi, "Compact and Efficient Bipolar Coupler for Wireless Power Chargers: Design and Analysis," in IEEE Transactions on Power Electronics, vol. 30, no. 11, pp. 6130-6140, Nov. 2015.

[2] K. Colak, E. Asa, M. Bojarski, D. Czarkowski and O. C. Onar, "A Novel Phase-Shift Control of Semibridgeless Active Rectifier for Wireless Power Transfer," *IEEE Transactions on Power Electronics*, vol. 30, no. 11, pp. 6288-6297, Nov. 2015.

[3] G. A. Covic and J. T. Boys, "Modern Trends in Inductive Power Transfer for Transportation Applications," *IEEE Journal of Emerging and Selected Topics in Power Electronics*, vol. 1, no. 1, pp. 28-41, March 2013.

[4] A. Tejeda, C. Carretero, J. T. Boys, and G. A. Covic, “Ferrite-less circular pad with controlled flux cancelation for EV wireless charging,” *IEEE Transactions on Power Electronics*, vol. 32, no. 11, pp. 8349–8359, Nov 2017.

[5] S. Ahn and J. Kim, “Magnetic field design for high efficient and low EMF wireless power transfer in on-line electric vehicle,” in Proceedings of the 5th *European Conference on Antennas and Propagation* (EUCAP), April 2011.

[6] SAE J2954. *Task Force on Wireless Power Charging*. [Online]. Available: http://www.sae.org

[7] A. Foote and O. C. Onar, "A review of high-power wireless power transfer," *IEEE Transportation Electrification Conference and Expo (ITEC)*, Chicago, IL, 2017

[8] *Guidelines for Limiting Exposure to Time-Varying Electric and Magnetic Fields (1 Hz to 100 kHz)*, Neuherberg, Germany, 2010.

[9] S. Kim, H. H. Park, J. Kim, J. Kim, and S. Ahn, "Design and analysis of a resonant reactive shield for a wireless power electric vehicle," *IEEE Transactions on Microwave Theory and Techniques*, vol. 62, no. 4, pp. 1057–1066, April 2014.

[10] D. Graovac, M. Pürschel, and A. Kiep, "MOSFET Power Losses Calculation using The Datasheet Parameters", *Infineon Application Note*, pp. 1-23, July 2006.

[11] P. S. Y. Xiong, S. Sun, H. Jia, and Z. J. Shen, "New Physical Insights on Power MOSFET Switching Losses", *IEEE Transactions on Power Electronics*, vol. 24, no. 2, pp. 525-531, 2009.

[12] A. K. Agarwal, "An Overview of SiC Power Devices", *2010 International Conference on Power Control and Embedded Systems*, pp. 1-4, 2010.

[13] M. Mohammad, S. Choi, Z. Islam, S. Kwak and J. Baek, "Core Design and Optimization for Better Misalignment Tolerance and Higher Range of Wireless Charging of PHEV," *IEEE Transactions on Transportation Electrification*, vol. 3, no. 2, pp. 445-453, June 2017.

[14] D. Patil, M. K. McDonough, J. M. Miller, B. Fahimi and P. T. Balsara, "Wireless Power Transfer for Vehicular Applications: Overview and Challenges," *IEEE Transactions on Transportation Electrification*, vol. 4, no. 1, pp. 3-37, March 2018.

[15] W. Li, H. Zhao, J. Deng, S. Li and C. C. Mi, "Comparison Study on SS and Double-Sided LCC Compensation Topologies for EV/PHEV Wireless Chargers," *IEEE Transactions on Vehicular Technology*, vol. 65, no. 6, pp. 4429-4439, June 2016.